

## Electronic Structure of Carbon Nanotubes

L.G.Bulusheva, A.V.Okotrub, D.A.Romanov<sup>†</sup>, D.Tomanek<sup>‡</sup>

*Institute of Inorganic Chemistry SB RAS, Novosibirsk, Russia*

<sup>†</sup>*Institute of Semiconductor Physics SB RAS, Novosibirsk, Russia*

<sup>‡</sup>*Department of Physics and Astronomy,  
Michigan State University, East Lansing, USA*

*(Received 3 December 1997, accepted for publication 15 December 1997)*

A study of the electronic structure of carbon nanoparticles has been carried out using the methods of quantum chemistry and X-ray emission spectroscopy. Fragments of  $(n,0)$  tubes with  $n = 6, \dots, 11$  and of  $(5,5) - (10,0)$  tubes were calculated using PM3 method. The dependence of the electronic structure of the fragment on length and symmetry was investigated. The structure of the frontier orbitals was shown to change regularly depending on the tube chirality. Band structure of  $(n,0)$  and  $(5,5)$  tubes was studied by the tight-binding method. A comparison of the basic blocks of the molecular orbitals (MOs) of the fragment and bands of  $(6,0)$  and  $(5,5)$  tubes was carried out. Experimental  $CK\alpha$  spectra for single-wall and multiwall carbon nanotubules were obtained. These spectra agree satisfactorily with the theoretical spectra plotted as the results of cluster calculations. The structure of the valence zone for the central hexagons of the nanotube fragments keeps the basic features in the series of tubes of various chirality. At the same time a considerable change of the electronic state of the boundary carbon atoms is observed.

### 1. Introduction

Carbon nanotubes are interesting as new nanosizing materials. It is proposed that defect-free nanotubes possess unique mechanic, electronic and magnetic properties, depending on diameter and chirality of tubes and also on the number of concentric shells in multiwall nanotubes. These materials can be practically used as molecular wires, catalytic supports, molecular adsorbents, etc. From the theoretical viewpoint, carbon nanotubes are interesting as an example of quasi one-dimensional structures, which are available for computer simulation and calculation.

Microscopic studies of the inner part of the deposit producing on the cathode of the carbon arc in the process of fullerene synthesis revealed the presence of

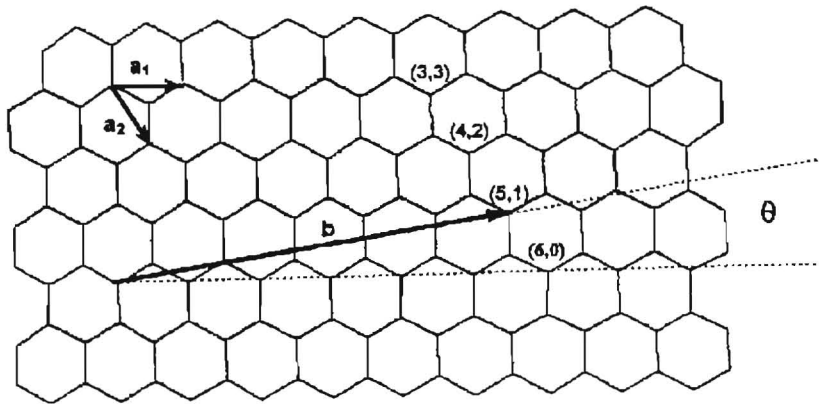


**Figure 1.** The graphene sheet and the base reference system suitable for description of the nanotube folding.

thin filaments of graphite with a length up to 10 000 Å, which were named carbon nanotubes [1]. Multiwall particles are from 1.5 nm to several dozens nm in diameter and consist of concentric tubes, whose number is varied from 2 to 50. The interlayer distance between concentric shells ranges from 3.4 Å [2] to 3.62 Å [3] depending on diameter of multiwall nanotube. Carbon hexagons are helically arranged on each graphitic tubule. The helical pitches vary from one shell to another. Measured angle of a separated tube ranges from 0° to 12° [3,4]. It is proposed that a tube growth proceeds until its end is kept open. When, for some reasons, several isolated pentagons are formed on a tube end, a tube is capped and its growth is stopped.

It was initially proposed that carbon nanotubes can be produced only when electric field is present. However, the methods of pyrolytic production of tubes were later elaborated [5]. Directed stream of carbon atoms results in precipitation of atoms on the support (quartz, ceramics, graphite) in the form of tubes forming the fibrous structure. It is suggested that fragments of fullerene-like structures as semi-spheres are being formed on the support after some time. Highly energetic carbon particles subside on the ends of these clusters, lengthening their walls continuously [6].

Carbon materials consisting of single-wall tubes are collected on the arc chamber inner wall under definite composition of the gas phase [7]. These tubes have chiral structure and diameter from 0.7 to 2.5 nm. Single-wall tubes were also synthesized by laser vaporization and further condensation of a carbon-nickel-cobalt mixture [8]. Disorderly orientated tubes with diameter from 10 to 20 nm forming ropes of tubes with equal diameter were produced as well. In the tubes composing the crystal-like ropes, two carbon-carbon bonds in the

hexagons are directed perpendicularly to the tube axis [9]. In the notation of Ref.[10], these tubes were assigned to nonchiral (10,10) configuration [11]. Conduction of these tubes was shown to be metallic [12]. It is proposed that the nickel and cobalt atoms diffusing on a tube end catalyze the tube growth [13].

Electronic properties of carbon nanotubes have been first considered in the framework of the model of “folded zone” [14]. In this model a carbon nanotube is represented by a cylinder produced by rolling of a graphite sheet. Diameter and chirality of this cylinder are determined by two integers  $n$  and  $m$ . Let us connect two points on the graphite sheet, which will be equivalent in the tube, by vector  $\mathbf{b}$  (Fig.1). This vector is the sum of the unit vectors of the graphite sheet:  $\mathbf{b} = n\mathbf{a}_1 + m\mathbf{a}_2$ . When  $n = m$ , chiral angle  $\theta$  is equal to  $30^\circ$ , two bonds in hexagons are perpendicularly directed to the tube axis and armchair  $(n, n)$  tubes are formed. When  $n$  or  $m$  are equal to zero, chiral angle  $\theta$  is equal to  $0^\circ$ . At the same time two bonds in hexagons are axially directed and zigzag  $(n, 0)$  tubes are formed. The tubes of these types are nonchiral tubes. Rolling of the graphite sheet at an angle  $0^\circ < \theta < 30^\circ$  gives a chiral tube. The model of “folded zone” suggests a simple recipe to obtain the basic features of the tube band structure by cyclic quantization of the graphene sheet quasi-momentum component corresponding to the electron motion along the tube circumference. The quantization condition defines an array of equidistant lines in the hexagonal Brillouin zone of the graphene sheet. These lines are parallel to the tube axis, and each of them corresponds to the one-dimensional subband. The valence and conduction bands of the graphene sheet are known to “touch” at the corners of the hexagonal Brillouin zone, often labeled as the  $K$ -point. The gap between the valence and the conduction band is proportional to the distance from the  $K$ -point in its vicinity. In the case of  $(n, n)$  tubes for any  $n$ , one line from this set passes always through the point  $K$ , and, therefore, such tubes must be metallic. For  $(n, 0)$  tubes, only when  $n$  is a multiple of three some lines from the set can pass near the point  $K$  and these tubes must have the zero gap like in graphite. All other  $(n, 0)$  tubes will be semiconductors. However, with the growth of the tube diameter, the tubes become more two-dimensional and the gap in semiconductor tubes decreases [15].

Later, these conclusions were supported by the tight-binding and local density approximation (LDA) calculations for infinite tubes [16]. As a result of (5,5) tube calculation by LDA method [17] it was determined that  $a_1$  and  $a_2$  bands cross at the Fermi level at  $k \sim 2\pi/3$ . These bands near the Fermi level consist of predominantly  $p$ -orbitals tangentially directed to the tube surface, similar to  $\pi$ -states in graphite. It was predicted that the tubes of this structure would be metallic. Calculated density of conduction electrons for the set of

these tubes was found to be close to the values which are characteristic of metals. This means that a material composed from these tubes must possess high electric conductivity. Band structures of  $(n,0)$  tubes with  $n$  from 6 to 9 were investigated by the tight-binding and LDA methods in Ref.[18]. The highest occupied and lowest unoccupied states for these tubes are doubly degenerate. The value of the gap from the LDA calculation is less than that obtained from the tight-binding calculation, but this difference diminishes with the increase in the tube radius. Comparison of the energy of the tube with that of the graphite belt, obtained by cutting the tube along its cylindrical axis, was performed in Ref.[19]. A critical radius for which the energy of the tube exceeds that of the belt was shown to be  $\sim 3 \text{ \AA}$ . The results of the LDA calculations showed that the effects of  $\pi^* - \sigma^*$  hybridization were developed for the tubes of small radii. These effects will considerably change the band structure of the tube comparing to that obtained in the "folded zone" model.

In order to describe the state of individual atoms and to get chemically significant information, it seems more natural (and more correct) to use quantum-chemical methods, which are particularly suitable for determination of the local properties of the investigated system. These methods were originally designed to describe finite systems. So, any extension of the obtained results to the case of an infinite system faces certain difficulties and must be performed with care. In particular, one has to properly choose the representative cluster and to separate bulk from surface effects in the results. Cluster methods allow us to study the electronic structure of the real physical objects, in particular, to estimate how the surface of a cluster affects its reactivity and electrophysical properties.

In the present work we present the results of the study of the electronic structure of  $(n,0)$  carbon nanotubes, where  $n = 6 - 11$ , and  $(5,5) - (10,0)$  nanotubes. A comprehensive investigation includes quantum-chemical calculations of the fragments of these tubes as well as infinite ones and X-ray emission spectroscopic study of carbon nanoparticles. Our objectives are the determination of electron interaction in the valence zone of the nanoparticles and interpretation of the X-ray spectra; establishment of the correlation between the results of cluster and crystal calculations of the carbon nanotubes; clarification of the influence of the boundary electron states on reactivity and growth of the nanotubes.

## 2. Methods and approaches

Quantum-chemical calculations of nanotube fragments have been performed using the MNDO semiempirical method [20], which belongs to the group of SCF-MO-LCAO methods. In this method, only valence electrons are taken into account, and three- and four-center integrals are omitted. Making use of the

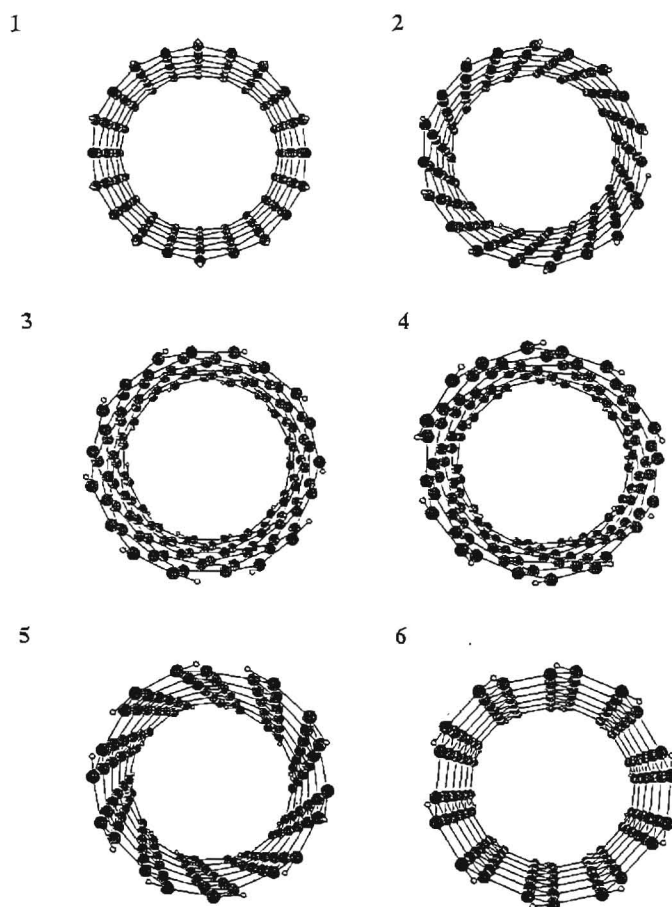


**Figure 2.** Structure of the calculated clusters of the tubes (10,0) - 1, (9,1) - 2, (8,2) - 3, (7,3) - 4, (8,2) - 5, (5,5) - 6. The perspective front view.

spatial anisotropy of  $p$ -orbitals in two-electron integral calculations, this method allows to describe correctly the repulsion of lone electron pairs. The choice of the phenomenological parameters on the basis of experimental data helps to automatically include correlation effects. Calculations were carried out using PM3 parametrization [21] and the GAMESS package [22]. The SCF convergence criterion was  $10^{-8}$  for total energy changes and  $10^{-5}$  for charge density changes between two subsequent cycles.

The structures of the fragments of (10,0) – (5,5) carbon nanotubes are shown in Fig.2. The (10,0) and (5,5) nanotubes have nonhelical structures, and the complete set of the tubes between these special cases is presented by chiral tubes. The dangling bonds at the ends of the nanotube fragments were saturated by

tube	(10,0)	(9,1)	(8,2)	(7,3)	(6,4)	(5,5)
diameter (Å)	7.88	7.55	7.27	7.06	6.93	6.88
chiral angle (°)	0.	6.46	12.75	18.75	24.35	30.

**Table 1.** Diameters and chiral angles of (10,0) – (5,5) tubes.

hydrogen atoms. In the calculations, all carbon-carbon bonds were assumed to be of the same length 1.42 Å. The distance between third neighbor carbon atoms along the tube circumference is 2.43 Å, between the carbon atoms and hydrogen atoms is 1.1 Å. All atoms in each calculated cluster are located on the circumferences of the to be determined diameters. This assignment of the cluster geometry ensures minimal distortion of the spatial structure for hexagons from ( $n, 0$ ) tube to ( $n, n$ ) tube. The calculated diameters and chiral angles for considered tubes are presented in Table 1.

Band structure calculations of carbon nanotubes were performed using the tight-binding Hamiltonian, with the universal set of the first and second nearest neighbor hopping integrals which reproduce various carbon structures, including graphite [23]. X-ray spectroscopic measurements were carried out for two samples: multiwall carbon nanoparticles (1) and single-wall closed carbon nanoparticles (2). The investigated samples were produced in the process of arc evaporation of graphite on the set-up described in Ref.[24]. Sample 1 is the inner part of the deposit that consists of  $\sim 20\%$  nanotubes, carbon cones and onions [25]. Sample 2 is obtained by the procedure described in Ref.[26] from the soot formed on the cold walls of the reaction chamber. It contains 100% of short single-wall carbon nanotubules.

CK $\alpha$  fluorescent spectra of samples 1 and 2 were recorded on X-ray spectrometer “Stearat”. The samples were deposited on the copper substrate and cooled to the liquid nitrogen temperature in the vacuum chamber of X-ray tube. The working regime of X-ray tube with the copper anode was  $U = 6$  kV,  $I = 0.5$  A. The spectra were recorded with  $\sim 0.5$  eV resolution. Single crystal NAP was used as a crystal-analyzer. The peculiarities of the use of this crystal for recording of CK $\alpha$  spectra have been described in Ref.[27]. The accuracy of determination of the energies of X-ray bands was  $\sim 0.3$  eV.

The energy position and intensity of a separate line in the X-ray spectrum of a compound can be directly compared with the results of quantum-chemical calculations. Methodological bases of interpretation of X-ray emission spectra in the framework of the MO LCAO method and of the Kupman’s theorem have

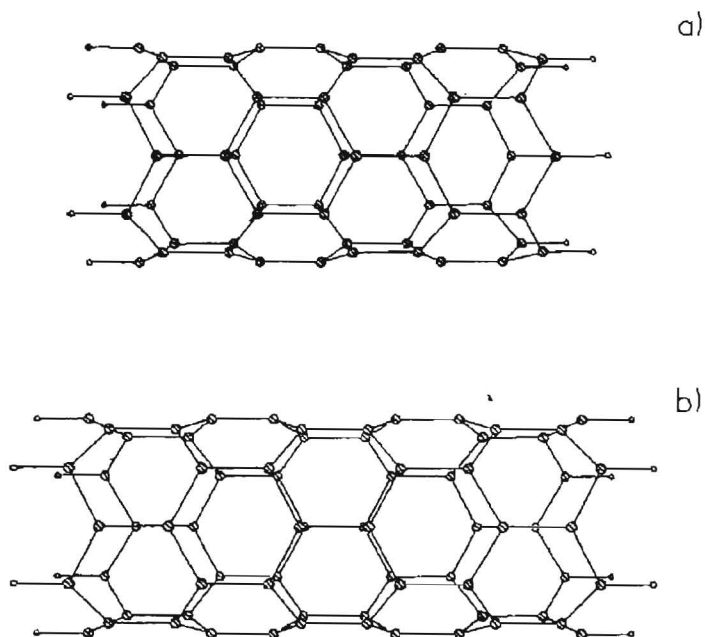


**Figure 3.** (6,0) tube clusters of  $D_{6d}$  (a) and  $D_{6h}$  (b) symmetry.

been developed in works [28]. Theoretical  $CK\alpha$  spectra of the carbon nanotubes were plotted on the basis of the calculations of nanotube fragments. A single line in a spectrum is proportional to the sum of squares of coefficients with which atomic orbitals (AOs) of carbon atoms participate in the formation of a specific MO of the cluster. The location of this line on the energy scale corresponds to the energy of the MO. Normalization of the lines was performed. Each line was described smeared by a Lorentzian curve with the width of 0.6 eV. The sum of all curves gives the resulting theoretical spectrum, which is afterwards compared with the experimental  $CK\alpha$  spectrum.

### 3. Choice of the representative cluster

The study of the dependence of the electronic structure of carbon nanotube fragments on their size was performed for the clusters of the (6,0) tube. This tube seems to have the lowest experimentally realizable diameter [10]. On the other hand, at the present time the calculations of relatively “long” clusters are only possible for the tubes of small diameters. We considered (6,0) tube fragments of different length. The point symmetry group of the (6,0) nanotube fragment is determined by the number  $N$  of carbon hexagons along the tube axis. Nanotube fragments with odd  $N$  belong to the group  $D_{6h}$ , whereas nanotube

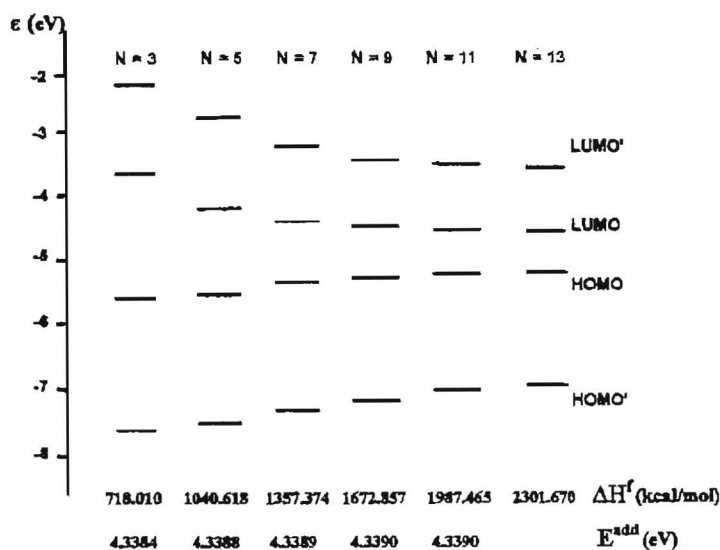
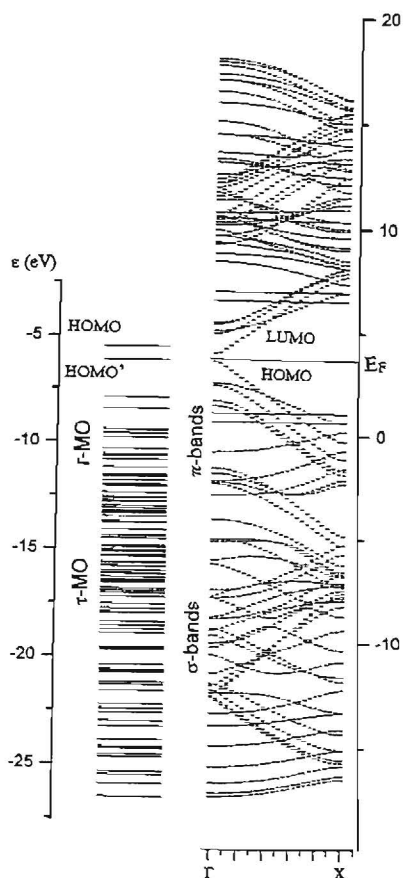


Figure 4. Calculated energy of frontier orbitals, the heat of formation ( $\Delta H_f$ ), and the energy required to join an additional carbon atom ( $E^{add}$ ) to fragments of the (6,0) tube with  $N$  hexagons in the axial direction.

fragments with even  $N$  belong to the group  $D_{6d}$  (Fig.3).

We calculated nanotube fragments with  $N = 3, 5, 7, 9, 11$ , and 13. Our results for the heat of formation of the nanotube fragments, the energy required to adsorb an additional carbon atom at the edge, and the energies of the frontier orbitals, are presented in Fig.4. The considerable energy difference between the nanotube fragments with  $N = 3$  and  $N = 5$  is caused by the fact that in the former case the boundary atoms affect strongly the central part of the nanotube fragment. The energy required to incorporate an additional atom remains practically constant between  $N = 9$  and  $N = 13$ . The obtained numerical results allow us to figure out the screening length of the tube end defects that affect the local electronic structure inside the tube. This length corresponds to four hexagons. Therefore, the nanotube fragment with  $N = 9$  is quite sufficient for modeling the energetic characteristics of an infinite tube.

From the results of calculations of the (6,0) tube by different methods, the energy gap changes from 0.2 to  $-0.83$  eV [18]. The cluster calculations overestimate the fundamental gap (Fig.4). The increase in the fragment size reduces the gap. However, changes in the HOMO-LUMO gap diminish fast with the increase in the fragment size, and become negligibly small when comparing this quantity in  $N = 11$  and  $N = 13$  tube fragments. We expect the gap to be  $\sim 1-3$  eV in the very large tube fragments and cannot compare directly this value to the width of the fundamental gap obtained from the band structure calculations.



**Figure 5.** Comparison between the occupied levels of the (6,0) tube fragment with  $N = 13$  hexagons in axial direction (left) and band structure of the (6,0) tube (right).

The conduction properties of nanotubes cannot be predicted from the results of cluster calculations. The comparison of the tight-binding result for the (6,0) tube and the result of PM3 calculation of the (6,0) nanotube fragment with  $N = 13$  is shown in Fig.5. The occupied molecular levels of the nanotube fragment formed from  $2p$ -AOs of carbon atoms are presented on the left-hand side. These molecular orbitals can be separated into two basic blocks. The block consisting of  $r$ -orbitals (these orbitals are directed perpendicularly to the tube axis) lies at higher energy. The other block, consisting of  $\tau$ -orbitals (these orbitals are tangentially directed to the tube surface), lies at lower energy. The dispersion curves  $E(k)$  for occupied energy bands formed from  $2p$ -AOs of carbon atoms are drawn in the right part of Fig.5. The bands are also clearly divided into two

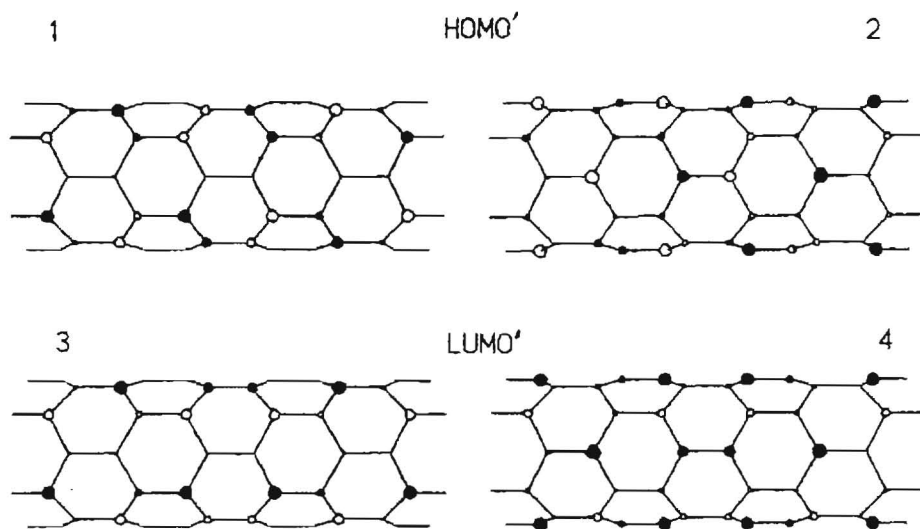


**Figure 6.** Structure of the HOMO' and LUMO' of the  $D_{6h}$  cluster of the (6,0) tube. We show the fragment surface turned to us. White circles denote AOs directed toward the tube axis, black circles represent AOs directed outward. Relative sizes of the circles correspond to the  $2p$ -AOs contributions to the orbital.

blocks, the block of  $\pi$ -bands and the block of  $\sigma$ -bands. The corresponding band widths are well correlated with the widths of  $r$ - and  $\tau$ -orbital energy blocks. Fig.5 shows that the energy level corresponding to the HOMO of the nanotube fragment has no counterpart in the infinite (6,0) tube. We must exclude this level from our discussion when comparing the results of cluster and band structure calculations. The HOMO structure of the nanotube cluster is presented by the contributions of AOs of the boundary carbon atoms and the similar wave functions cannot be constructed as a result of the infinite tube calculation. The spatial structure of the LUMO' ( $e_{2g}$ ) and HOMO' ( $e_{2u}$ ) orbitals corresponds to the structures of Bloch wave functions of the occupied and unoccupied  $\pi$  bands near the Fermi level. We showed the structure of these  $r$ -orbitals for carbon atoms at the fragment surface in Fig.6. The size of the circles is proportional to the contributions of  $2p$ -AOs to the orbital. The black circles represent positive phase and the white circles negative phase of wavefunction. The HOMO' and LUMO' sets contain one orbital component with clearly visible strip character (Figs.6.1 and 6.3). We find four strips containing carbon atoms which have zero contribution to their charge density from these orbitals. The chains of carbon atoms between these strips contain atoms on which these states are predominantly localized. The analysis of the electronic structure of the (6,0) nanotube

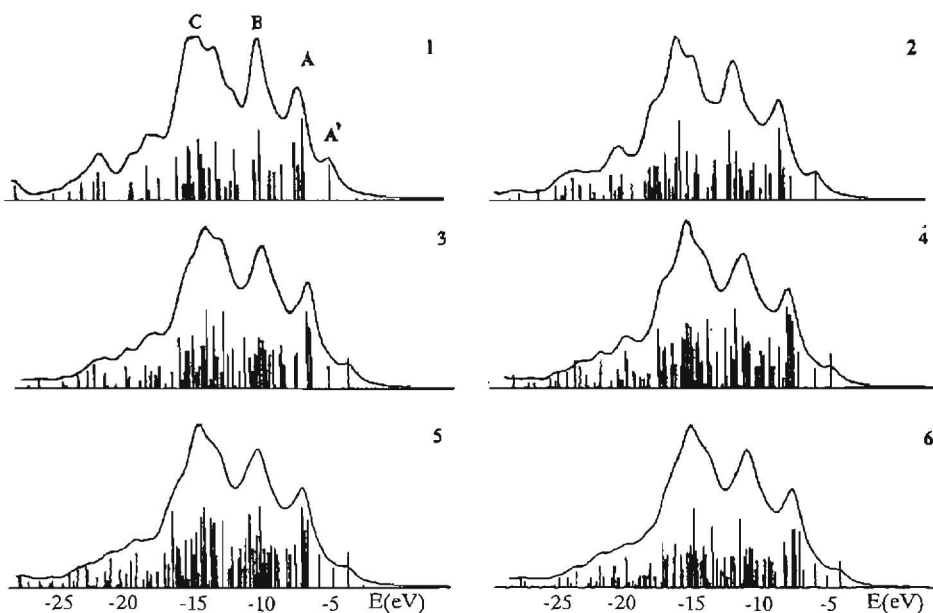


**Figure 7.** Theoretical CH $\alpha$  spectra for central carbon atoms of clusters of different lengths ( $N$  hexagons) of the (6,0) tube: 1 -  $N = 3$ , 2 -  $N = 5$ , 3 -  $N = 7$ , 4 -  $N = 9$ , 5 -  $N = 11$ , 6 -  $N = 13$ .

fragments demonstrates that the fragment with  $N = 5$  already shows the strip structure in molecular orbitals. Consequently, this cluster size is sufficient to discuss quantitatively the character of electron wave functions in the infinite tube.

Dependence of the distribution of  $2p(C)$  electron density in the valence zone of the cluster on its length is presented in Fig.7. Theoretical CK $\alpha$  spectra are plotted for the central hexagons of the calculated cluster of the (6,0) tube. The shapes of the spectra for the fragments with  $N = 9, 11$  and  $13$  are practically identical. But the theoretical spectrum for the cluster with  $N = 5$  is already characterized by the main particularities preserved in the spectra of the longer clusters. Thus, the relative intensities of the A', A, B and C maxima and the distances between them nearly do not change. Hence, the theoretical X-ray spectrum which is used for the interpretation of the experimental spectrum and for the investigation of the electronic structure of the tube can be constructed as a result of the calculation of the tube fragment with five hexagons in length.

It is usual in self-consistent calculations to estimate the accuracy of the wave functions and corresponding energies. The solution of the Hartree-Fock equation is regarded as self-consistent if for two consecutive iterations the variation of the total energy of the system is less than a given (small) quantity  $\delta$ ,

whereas the variation of the charge density is less than another quantity  $\delta'$ . In the calculations of the (6,0) tubes with even-numbered  $N$  (i.e. for tube fragments of  $D_{6d}$  symmetry) we could not achieve charge density convergence for  $\delta' < 10^{-2}$ . Consequently, the quality of our wavefunctions is not sufficient for quantitative discussions. A more detailed examination shows that the LUMO and HOMO of these nanotube fragments are energetically degenerate and belong to the irreducible representation  $e_3$ . In other words, the HOMO of these nanotube fragments proves to be half-occupied. The mentioned LUMO and HOMO, as well as these orbitals in  $D_{6h}$  nanotube fragments, consist mainly of  $2p$ -AOs of the edge atoms. By virtue of the symmetry operations of the point group  $D_{6d}$ , such orbitals have to be doubly degenerate. The total number of electrons in the system is not sufficient to fill this orbital completely. The unpaired spins result in a net dipole moment and prevent the self-consistent calculation from converging. However, adding two extra electrons to the system (e.g. by intercalation) results in zero net dipole moment for the completely filled HOMO, and the self-consistent computation converges. From this consideration we can conclude that the charge-neutral nanotube fragments of  $D_{6d}$  symmetry are unstable. We would, however, expect a stabilization of this system by a symmetry-lowering Jahn-Teller distortion. The structure of the HOMO' and LUMO' orbitals in nanotube fragments of  $D_{6d}$  symmetry appears to be similar to that of  $D_{6h}$  nanotube fragments.

From the investigation performed the choice of the size of clusters is dependent on the studying aspect of the electronic structure of carbon nanotubes. The thermodynamic characteristics of nanotubes can be estimated from the calculation of the fragment not less than nine hexagons in length. A fragment with five hexagons in length is sufficient for the study of the MO structure, reactivity and the electron density distribution in the valence zone of carbon nanotubes.

#### 4. Electronic structure of $(n,0)$ nanotubes

To study the dependence of the electronic structure of  $(n,0)$  tubes on the number of hexagons along their circumference, we considered nanotube fragments with the same number of hexagons in the axial direction. For the latter quantity we used  $N = 5$ , i.e. we considered nanotube fragments of  $D_{nh}$  symmetry. We performed quantum-chemical calculations for  $(n,0)$  nanotube fragments with  $n = 6, \dots, 11$ . Electron level diagrams for these clusters are presented in Fig.8. For all the considered  $(n,0)$  nanotube fragments the electron density of the HOMO and LUMO is localized on those carbon atoms at the edge that are connected to hydrogen atoms. In the fragments of (6,0), (8,0), and (10,0) nanotubes, the LUMO and HOMO prove to be nondegenerate. In fragments of

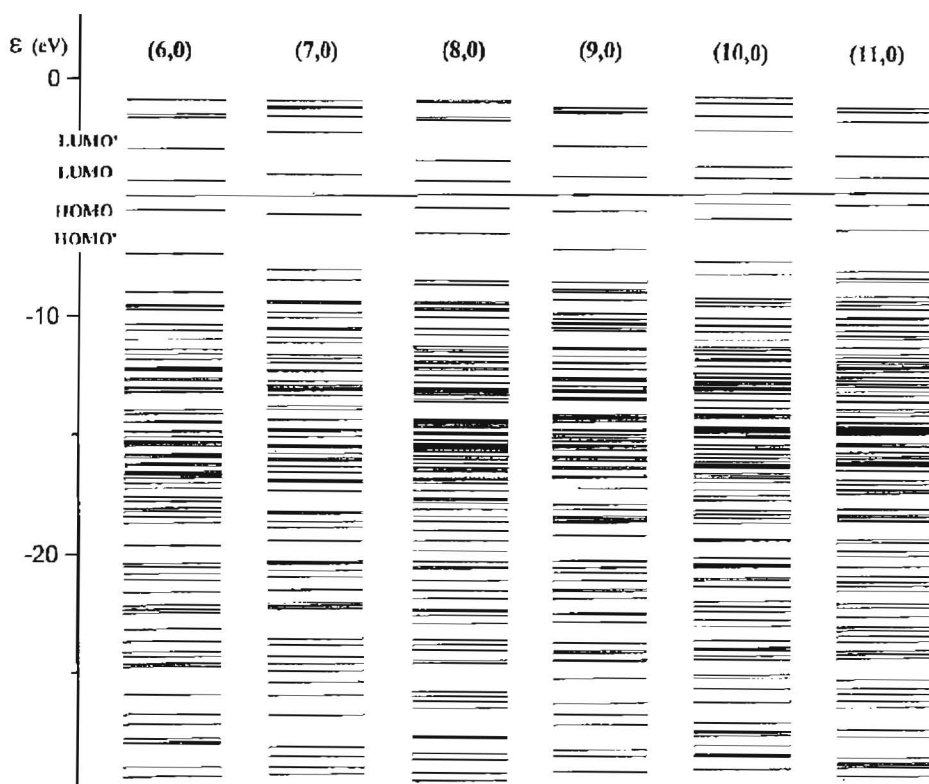


**Figure 8.** Electronic eigenvalues of clusters of the  $(n, 0)$  tubes, with  $n = 6, \dots, 11$ .

$(7,0)$ ,  $(9,0)$ , and  $(11,0)$  nanotubes, these orbitals are doubly degenerate. The latter fact seems to be caused by the fact that the number of hexagons along the tube circumference is odd. The HOMO' and LUMO' states in nanotube fragments of  $(6,0) - (11,0)$  tubes have doubly degenerate orbitals of  $r$ -type. The  $(n, 0)$  tubes we considered split naturally into two groups, namely tubes with the even number of hexagons along the tube perimeter (even  $n$ ) and tubes with the odd value of  $n$ . In tubes with both even-valued and odd-valued  $n$  (Fig.8), the energy gap between the HOMO' and the LUMO' decreases with increasing tube diameter, though the gap is larger in tubes with an odd-valued  $n$ . As we know from cluster calculations, the HOMO-LUMO gap correlates with the stability of the nanotube fragment. We conclude that tubes with an odd-valued  $n$  should be synthesized in a larger abundance under thermodynamically controllable conditions.

The dispersion curves of the  $(n, 0)$  tubes with  $n = 6, \dots, 11$  are shown in Fig.9. This tube family splits into three groups. The  $(3n, 0)$  tubes have vanishing energy gaps. The gap increases in  $(3n + 1, 0)$  and in  $(3n + 2, 0)$  tubes.

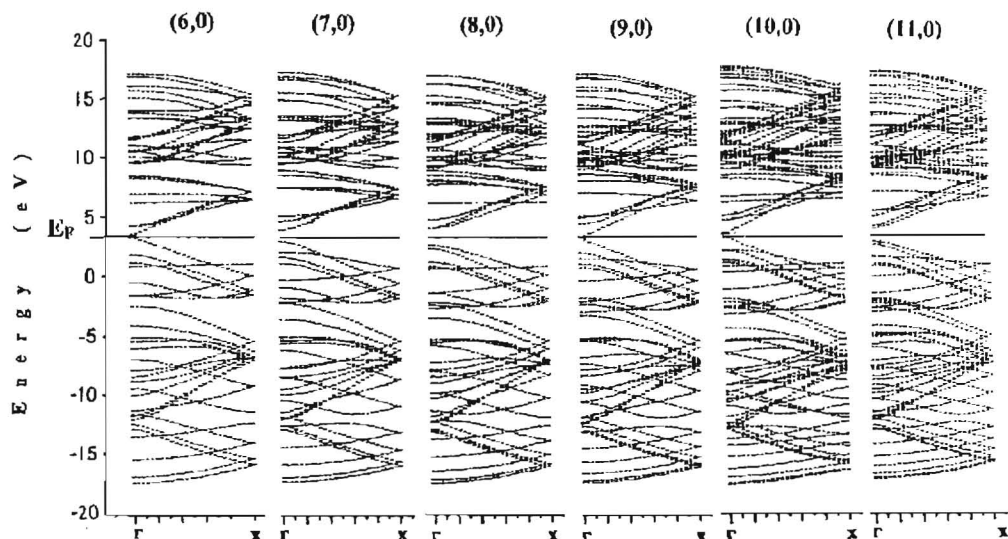


**Figure 9.** Band structures of the (6,0) - (11,0) nanotubes.

Consequently, (6,0) and (9,0) tubes are likely to show semimetallic conductivity, similar to graphite. HOMO's of infinite  $(n, 0)$  tubes are doubly degenerate and their structures are correlated with structures of the HOMO's of the fragments of these tubes. The HOMO's structures for the (7,0) - (11,0) tubes are shown in Fig.10. The character of the interaction between carbon atoms in the HOMO' of these tubes is similar to that of (6,0) tube. As in the latter case, we observe bonding between the pairs of atoms along the tube circumference, and antibonding between the pairs along the tube axis. Strips of carbon sites, which have zero contribution to their charge density from this MO, can be seen in each of the orbital components of the HOMO' set for the (7,0), (8,0), (10,0), and (11,0) tubes. For the (6,0) and (9,0) tubes, on the other hand, only one component of the HOMO' orbital set shows an obvious strip character. The strips in these tubes are distributed symmetrically, and all of them are half a hexagon wide. In (9,0) nanotube fragments, we observe six strips of carbon atoms with zero electron density which connect to chains, similar to the results discussed for the (6,0) tube.

### 5. Electronic structure of (10,0) - (5,5) nanotubes

The study of the dependence of the electronic structure of the carbon nanotubes on the helical picture of the hexagons was performed for a series of (10,0) - (5,5) tubes. Total energies of the tube clusters and the eigenvalues of HOMO

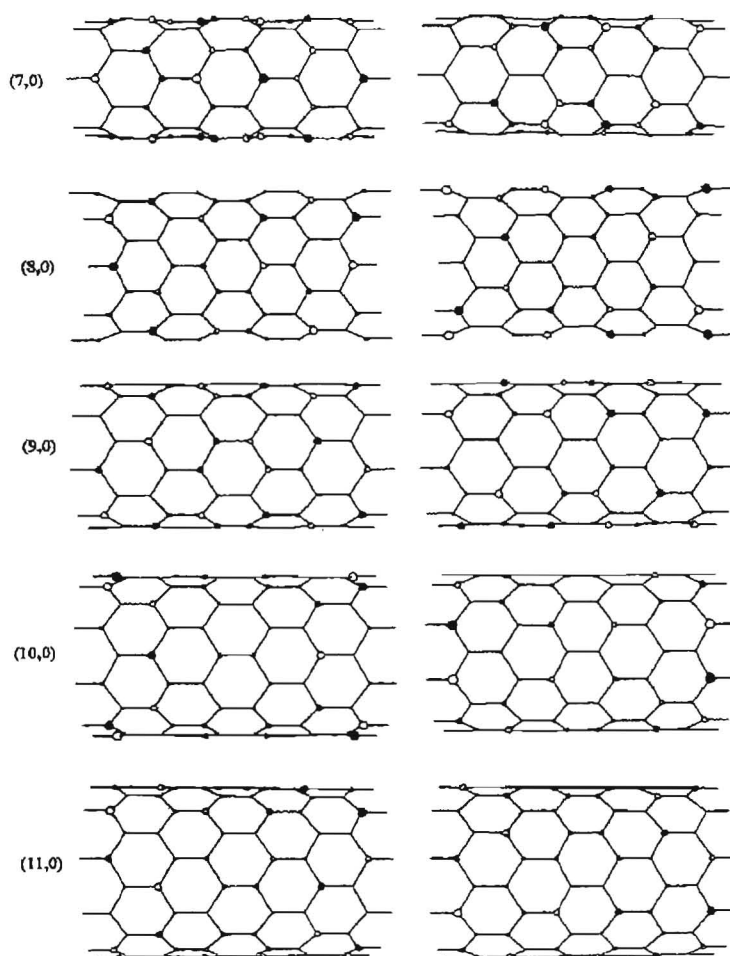


**Figure 10.** Structures of the HOMO's for the (7,0) - (10,0) tubes.

and LUMO are presented in Table 2. The theoretical  $CK\alpha$  spectra for the tubes were plotted on the forty central atoms. The comparison of these spectra with the experimental spectra of carbon nanoparticles is given in Fig.11. The shapes of the theoretical spectra are similar in general and satisfactorily agree with the experiment. The  $CK\alpha$  spectra of carbon nanoparticles look very similar to the ones of graphite [29]. The theoretical X-ray spectrum of two-dimensional graphite [30] also has much in common with our calculated spectra of the carbon nanotubes. Therefore, the electronic structure of nanotubes holds the principal features of the electronic structure of graphite filament in spite of the distortions of carbon hexagons under rolling of a graphite sheet into a tube.  $r$  and  $\tau$  orbitals of carbon nanotubes are analogous to  $\pi$  and  $\sigma$  orbitals of graphite.

The four principal features labeled by  $A'$ ,  $A$ ,  $B$ , and  $C$  can be identified

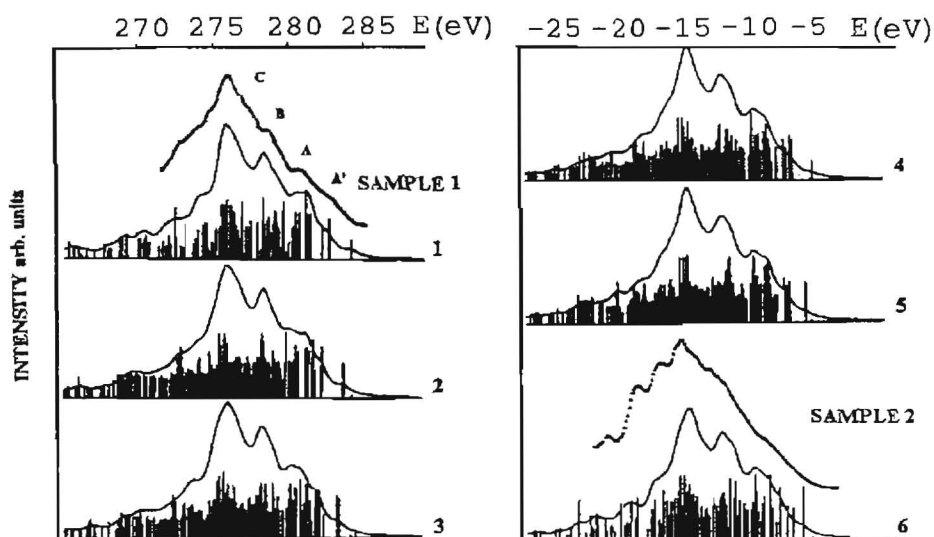
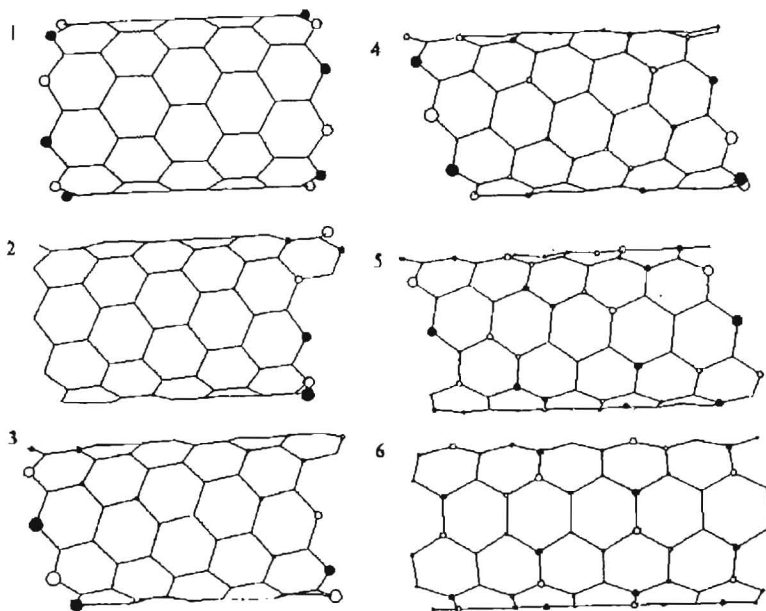


Figure 11. Theoretical  $CK\alpha$  spectra for central carbon atoms of clusters of tubes: (10,0) - 1, (9,1) - 2, (8,2) - 3, (7,3) - 4, (8,2) - 5, (5,5) - 6. Experimental  $CK\alpha$  spectra of samples 1 and 2.

tube	(10,0)	(9,1)	(8,2)	(7,3)	(6,4)	(5,5)
total energy (a.u.)	-532.94	-532.93	-532.94	-532.91	-532.77	-533.03
HOMO energy (eV)	-4.3	-3.9	-1.6	-4.2	-3.7	-3.4
LUMO energy (eV)	-5.4	-5.9	-5.6	-5.9	-6.5	-6.8
HOMO-LUMO gap (eV)	1.1	2.0	4.0	1.7	2.8	3.4

Table 2. Results of PM3 calculations of the tube fragments.

separated in the  $CK\alpha$  spectra of the carbon nanotubes. Depending on the tube configuration, the energy positions and relative intensities of these maxima are different in the theoretical spectra. From the comparison of the  $CK\alpha$  spectra of the samples 1 and 2 the relative decrease in A' maximum and the growth of B maximum in the spectrum of the single-wall tubules (sample 2) can be noticed. The multiwall tubules from the sample 1 are characterized by the chiral structure close to the  $(n, 0)$  one. The orientation of the carbon hexagons for the single-wall tubules composing the sample 2 was not determined. It may be assumed that the tubules which are synthesized in the gas phase by the arc vaporization method have the hexagon arrangement similar to that in the tubules synthesized by the laser ablation of graphite. As we noted above, the latter tubules have



**Figure 12.** Structures of the HOMOs in the clusters of the tubes: (10,0) - 1, (9,1) - 2, (8,2) - 3, (7,3) - 4, (8,2) - 5, (5,5) - 6.

the  $(n,n)$  structure. The observed differences in the experimental spectra are correlated with those in the theoretical spectra of the series of (10,0) – (5,5) tubes. The tendency of the growth of the B maximum and the approach of the energetic positions of the A, B and C maxima are observed in the spectrum of the (5,5) tube. Besides, the change of the position of the A' maximum in the theoretical spectra corresponds to the observed decrease of the intensity of the A' maximum in the spectrum of sample 2.

The comparison of the theoretical and experimental spectra allows us to interpret the experimental data and to investigate the electronic structure of the tubes having different chiralities. The short wave maximum A' in the spectra of (5,5), (6,4) and (7,3) tubes appears as the result of X-ray transitions from HOMO. Its intensity progressively decreases. HOMO is an  $r$ -orbital and the HOMOs structures for the calculated clusters are shown in Fig.12. If in the cluster of the (5,5) tube the electron density is regularly distributed over the central atoms, the relative decrease in the A' maximum and the increase in the B maximum in the spectrum of the single-wall tubules (sample 2) as on the boundary carbon atoms, the density is progressively localized on the periphery of the clusters of chiral tubes. In the cluster of (10,0) tube, all electron density is localized on twenty carbon atoms bonded with hydrogen atoms. The HOMOs

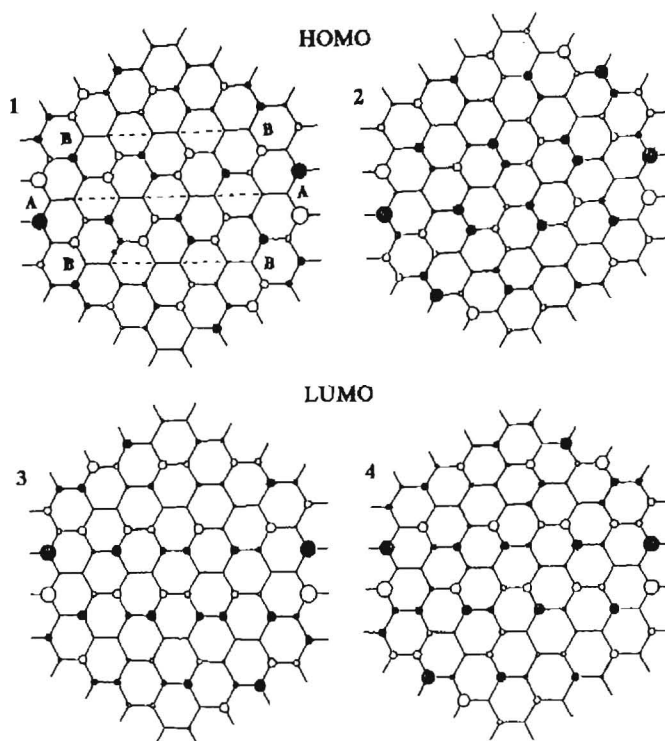


**Figure 13.** Structure of the HOMO and LUMO states in a graphite flake of  $D_{6h}$  symmetry.

structures for the clusters of (5,5) and (10,0) tubes are the extreme cases, and the HOMOs structures of the chiral tubes present the gradual transfer from one case to the other.

It can be suggested that the structures of the frontier orbitals of the tube clusters can be explained from the HOMO and LUMO structures of the cluster of graphite filament (Fig.13). The calculated cluster  $C_{96}H_{24}$  belongs to the  $D_{6h}$  point group of symmetry. HOMO (LUMO) of this cluster is a doubly degenerate orbital. Under rolling of a graphite filament into a tube, the cyclic operations of symmetry were imposed on the structures of these frontier orbitals. Additional conditions of symmetry, determining the structure of the orbitals, arise for the clusters with various boundaries.

From the comparison of the orbital structures presented in Figs.6 and 13 it can be concluded that the HOMO' (LUMO') structure of the cluster of (6,0) tube corresponds to the HOMO (LUMO) structure of the cluster of graphite. The structures of the wave functions of the frontier orbitals for the graphite filament have the period equal to three in the rolling direction for  $\theta = 0^\circ$ . For example,

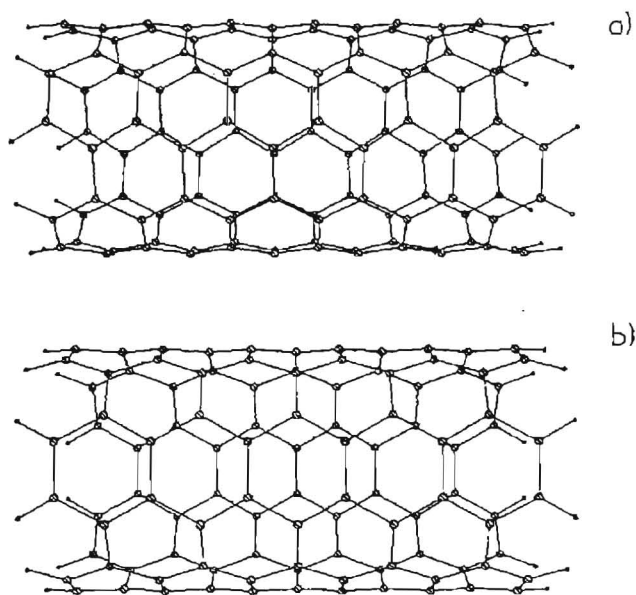
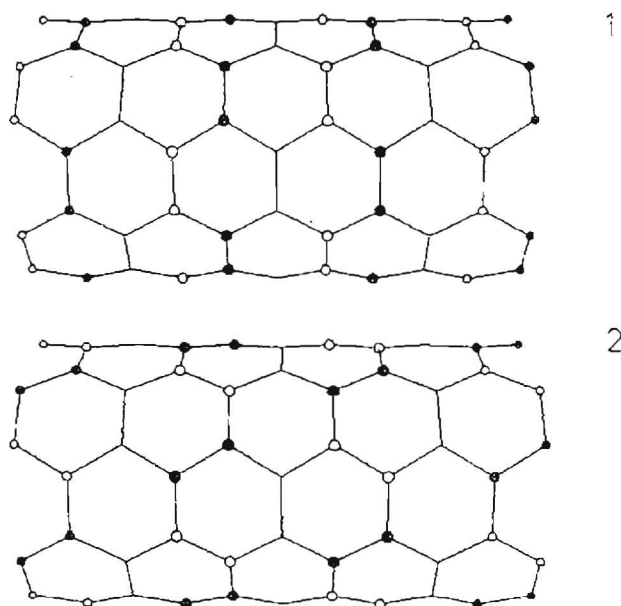


Figure 14. Calculated clusters of (5,5) tube of  $D_{5d}$  - (a) and  $D_{5h}$  - (b) symmetry.

the strip BB turns to itself through three hexagons for one of the components of the HOMO set (Fig.13(1)). Hence, the correspondence of the structures of the frontier orbitals of graphite and the clusters of carbon nanotubes was observed for all  $(n, 0)$  tubes for which  $n$  is a multiple of three. The existence of the orbitals with the strips of the zero charge density (similar to AA or BB strips) in the structure of MOs of graphite leads to the formation of the orbitals with the strips along the circumference tube. Indeed, the clusters of  $D_{nh}$  or  $D_{nd}$  symmetry point group possess the axis of  $n$ -fold rotation  $C_n$ , coinciding with the tube axis. As the result of the rotation around this axis, the atoms on the circumference of the tube are superimposed and, therefore, must have the same charge density. The structure of HOMO (LUMO) for the clusters of  $(n, 0)$  tubes is an example of this orbital with the localization of electron density on the boundary carbon atoms (Fig.11). These localized states appear only in cluster calculations and do not describe the electron properties of infinite tubes. On the other side, these orbitals are supposed to play a crucial role in the processes taking place at the ends of real nanotubules, such as tubule growth or oxidation.

The clusters of  $(n, n)$  tubes belong to the  $D_{nh}$  or  $D_{nd}$  symmetry point group, depending on the number of hexagons in the length of the cluster (Fig.14). HOMO (LUMO) structures of the clusters of different symmetries are different. The HOMO and LUMO structures for the  $D_{5h}$  cluster of the (5,5) tube are pre-



**Figure 15.** HOMO - 1 and LUMO - 2 structures in  $D_{5h}$  cluster of (5,5) tube.

sented in Fig.15. The strips of zero charge density along the tube circumference exist in both of these orbitals. The HOMO structure of the tube cluster corresponds to the structure of one of two components of LUMO of the graphite filament (the bonding between carbon atoms along the tube circumference and antibonding between a pair of carbon atoms along tubes are observed). The LUMO structure corresponds to the component of HOMO set for the graphite filament and has the opposite character of bonding for pairs of carbon atoms to the one for HOMO of this cluster. The HOMO (LUMO) structure of the cluster of  $D_{5d}$  symmetry (Fig.11) corresponds to the other component of LUMO (HOMO) of the graphite filament. The imposition of cyclic symmetry conditions on the structure of HOMO and LUMO of graphite filament leads to the increase (decrease) of antibonding HOMO (LUMO) and, hence, to the inversion of this orbitals.

The tight-binding result for (5,5) tube and the results of PM3 calculations of the nanotube fragment of  $D_{5d}$  symmetry are compared in Fig.16. We consider the orbitals with a considerable participation of  $2p$  AOs of carbon atoms. The occupied MO of clusters can be separated into three basic blocks. The block consisting of  $r$ -orbitals corresponds to the A' and A maxima in the X-ray spectrum, the block consisting of the orbitals corresponds to the B and C maxima and the third block consists of  $\tau$  MOs formed from both  $2p$  (C) and  $2s$  (C)-AOs. The energy gaps between the blocks of MOs are caused by the different character of

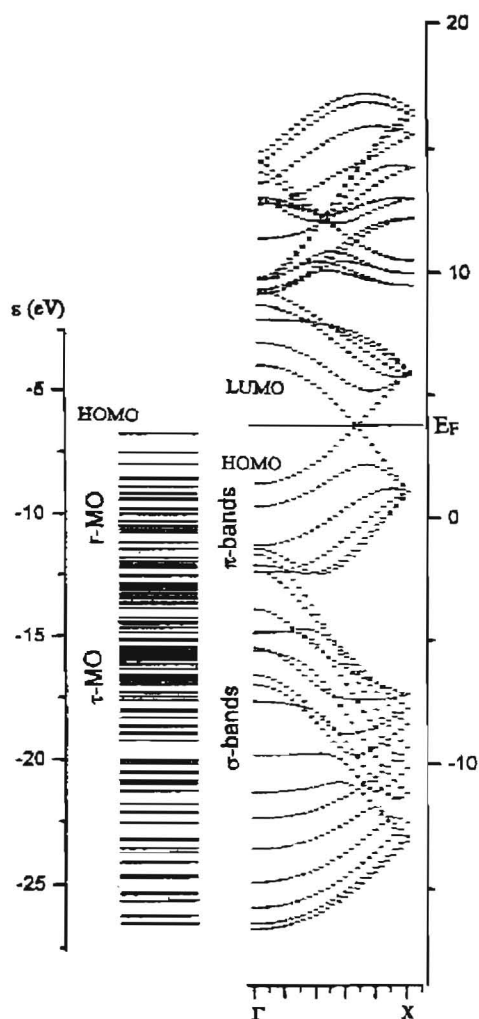


**Figure 16.** Correlation between the occupied levels of  $D_{5h}$  fragment (left) and band structure of (5,5) tube (right).

the electron interactions. The widths of these blocks of MOs are well correlated with the widths and the densities of states of the blocks of occupied bands of different symmetry.

A direct comparison of the band structure with the molecular levels by establishing the correspondence between the boundaries of the general blocks of MOs and of the bands of the same symmetry leads to close correspondence of HOMO level to the Fermi level. The highest occupied and lowest unoccupied bands of the (5,5) tube cross the Fermi level at the position roughly  $2/3$  in the Brillouin zone along  $\Gamma$ - $X$  direction. This inversion of the bands is consistent with the correlation of the HOMO (LUMO) structure for the clusters of (5,5) tube

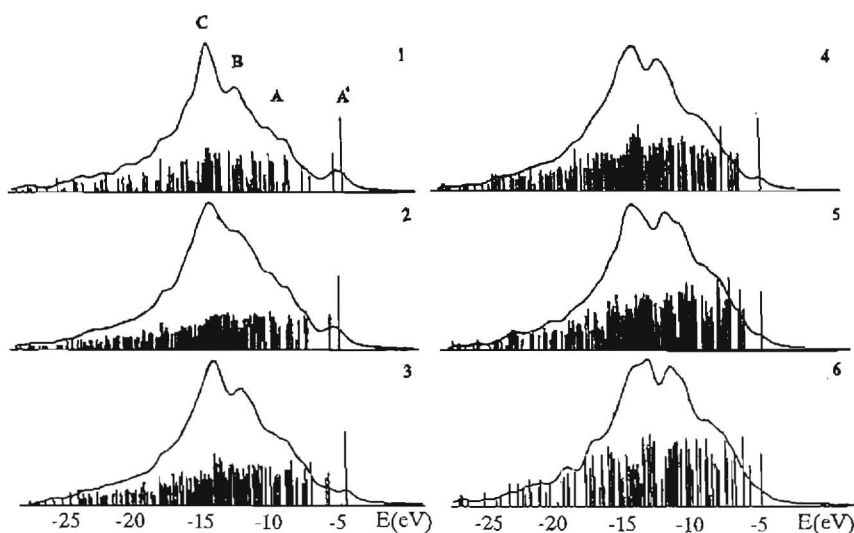


**Figure 17.** Theoretical  $CK\alpha$  spectra for boundary carbon atoms of clusters of tubes: (10,0) - 1, (9,1) - 2, (8,2) - 3, (7,3) - 4, (8,2) - 5, (5,5) - 6.

with the LUMO (HOMO) structure for the cluster of the graphite filament. The structures of HOMO and LUMO of the  $D_{5d}$  cluster correspond to the structures of the Bloch functions of the infinite (5,5) tube near the Fermi level.

The performed investigation shows that the peculiarities of the structures of the frontier orbitals of the clusters of nonchiral carbon nanotubes can be determined from the structure of HOMO (LUMO) of the graphite cluster. The distortions of the carbon hexagons under rolling of graphite sheet lead only to a small change of the relative contributions of  $2p(C)$ -AOs to the MOs.

The short wave maximum  $A'$  in the spectrum of (10,0) tube appears as a result of the X-ray transitions from HOMO. This doubly degenerate MO is also an orbital of  $r$ -type. The orbitals of the (9,1) and (8,2) tubes corresponding to the HOMO' of (10,0) tube and forming the  $A'$  maximum in spectra of these tubes split. The group of MOs forming the A maximum in the X-ray spectra of the nanotubes, occupies the energy range from  $-7$  to  $-11$  eV. These MOs are the orbitals of  $r$ -type. The group of MOs ( $\varepsilon \approx -11.3$  to  $-14.0$  eV) forming the B maximum consists of MOs as well of  $r$  type as of  $\tau$  type. In these MOs of  $\tau$  type the  $2p(C)$  AOs of the neighboring pairs of atoms are directed perpendicularly to the C-C bond.  $2p(C)$  AOs participate more noticeably in the construction of the MOs forming the C maximum ( $\varepsilon \approx -14.0$  to  $-17.0$  eV). These orbitals provide the  $\sigma$ -interactions between the carbon atoms. The maxima corresponding to higher energy bonds appear as a result of X-ray transitions from MOs

with a considerable contribution of  $2s(\text{C})$  AOs. It should be noted that a full correspondence, consistency of the experimental and theoretical spectra cannot be obtained, because the real samples have more complicated structure than the calculated models.

The clusters considered have the equal number of carbon and hydrogen atoms. But the boundary sizes for these clusters are considerably different, especially for the clusters of chiral and nonchiral tubes. As a result the obtained total energies for the clusters (Table 2) are inconsistent with the stabilities of the nanotubes. Extreme members of the tube series – (10,0) and (5,5) tubes may be an exception. The total energy of the cluster of the (5,5) tube is considerably lower than that of the cluster of the (10,0) tube. Hence the (5,5) tube is more thermodynamically stable than the (10,0) tube. Qualitatively, the relative stability of the clusters of various tubes can be deduced from the LUMO-HOMO gaps [31]. According to these data (Table 2) the tubes with metal conductivity, (5,5) and (8,2) tubes, are most stable. The calculated clusters can be considered as clusters having minimal size for the description of the electronic structure of nanotubes. The theoretical X-ray spectra of the central parts of the clusters are very similar; therefore the electronic states of the carbon atoms in the infinite tubes of different types are close to each other. The electronic states of the boundary carbon atoms are considerably different for the clusters of various tubes. This can be reflected in the theoretical X-ray spectra which are plotted for the fourth boundary carbon atoms (Fig.17). The ratio of the intensities of the A, B and C maxima is changed from the cluster of the (10,0) tube to the cluster of the (5,5) tube. The continuous decrease in the intensity of the A' maximum is connected with the change of the contribution of  $2p(\text{C})$ -AOs of the edge carbon atoms to the frontier MOs. Hence, the boundary of the clusters of various nanotubes will have the different reactivities.

## 6. Growth of carbon nanotubules

Carbon tubules observed in the carbon deposit of arc-discharge reactor have the atomic structure which is rather similar to that of  $(n, 0)$  tubules. The question of interest is, how the conditions of their synthesis, namely, the presence of electric field and high temperature (up to  $3000^\circ \text{C}$ ) affect the structure of grown tubules. From this viewpoint, our results for the frontier orbitals are most important. The frontier nature of these orbitals is twofold. Spatially, they are localized at the tube ends. On the energy scale, they occur inside the fundamental gap of the infinite tube. As discussed above, these orbitals are essentially different in the cases of tubes with the even and odd numbers  $N$  of hexagons along the tube axis.

In the tubes with odd-valued  $N$ , the frontier orbitals correspond to the HOMO and LUMO of infinite tubes. Consequently, the adsorption of carbon atoms (or atoms of other elements) takes place at the ends of the tube and results in net growth of the tube. However, as soon as one more layer (or ring) is completed at the tube end,  $N$  increases by one and becomes even. As discussed above, such tubes with even-valued  $N$  are unstable when charge-neutral, but become stable when carrying an excess charge of  $-2e$ . In the case of electron deficiency (the net electric charge being  $+2e$ ), the boundary states are absent, and the tubule reactivity decreases. We conclude that continuous growth of  $(n, 0)$  nanotubes requires a net excess charge, which could be provided from the cathode of the carbon arc apparatus, or by using alkali or alkali earth metals as catalysts.

Since carbon tubes are known to grow on the cathode during the carbon arc discharge process, the reasoning presented above should suggest the formation of  $(n, 0)$  nanotubes under these conditions. Indeed, the  $(n, m)$  tubes generated in this way are characterized by  $m$  typically much smaller than  $n$ , corresponding to a small chiral angle. The nonzero value of the chiral angle is linked to growth kinetics, since fastest growth is expected near the "step" at the growing edge. From the chemical viewpoint, the most interesting feature of the frontier orbitals is that they are of  $r$ -type. This means that these orbitals do not take part in the radical chemisorption reaction. Their role is nevertheless crucial, since they are associated with all the carbon atoms that adsorb at the entire surface of the tubule and then diffuse to either end. Thus, the very existence of the frontier orbitals makes the oxidation and chemical destruction processes take place at the tube ends.

Carbon tubules having the atomic structure  $(n, n)$  grow in gas phase under temperatures  $\sim 1200^\circ \text{C}$ . As our calculations have shown, the clusters of  $(n, n)$  tubes are most thermodynamically stable and this fact can explain the synthesis of these tubules at the temperatures lower than those of the synthesis of the tubules whose structure is close to  $(n, 0)$ . The  $(n, n)$  tubules grow by consistent alternation of the clusters of  $D_{nh}$  and  $D_{nd}$  symmetry. According to the calculations, the HOMO-LUMO gaps for these clusters are close, therefore the probabilities of the formation of the clusters of both structures are the same. Hence, the growth of the  $(n, n)$  tubules do not require external influences such as electric field. The catalytic role of the metal atoms (Co, Ni) is the reduction of the energy barrier of the connection of the carbon atoms which are necessary for the longing of the tubules.

## 7. Conclusion

The study of the electronic structure of  $(n, 0)$  carbon nanotubes by the cluster and crystal methods allow one to find out the regularity in the change of the structure of the frontier orbitals as the number  $n$  is changed. The electronic structure of the clusters of the nanotubes was shown to be determined by the parity of the number of the hexagons in the length of the tube and along the circumference tube. The  $D_{nd}$  clusters (with even number of the hexagons in the length of a tube) are thermodynamically unstable when its charge is neutral. We believe that the presence of carbon nanotubes with the structure close to that of the  $(n, 0)$  tubes results from the net negative charge provided by the cathode in the carbon arc. The HOMO structure of  $(n, 0)$  nanotube fragments depends on the symmetry of the fragment, but is localized on the edge atoms. This reactive frontier orbital is responsible for the tube growth resulting from carbon atoms adsorbed on the walls diffusing to and adsorbing on the exposed edge.

The comparison between the results of the band structure and cluster techniques shows that the occupied and unoccupied Bloch states of  $\pi$  character found near the Fermi level of  $(n, 0)$  tubes correspond to the HOMO's and LUMO's of carbon nanotube fragments. The HOMO' and LUMO' of  $(3n, 0)$  tube fragments correspond to the HOMO and LUMO of flat graphite flakes of  $D_{6h}$  symmetry, which is the reason for the metallic character of these tubes.

On the basis of cluster and crystal calculations of the  $(5, 5)$  tube it was shown that  $(n, n)$  tubes have metallic conductivity and are the most stable in the series of tubes of close diameter. The production of these tubes does not demand the presence of electric field and can be realized under the conditions of the hydrocarbon pyrolysis of the carbon soot formed by arc vaporization of graphite and by the laser ablation of carbon-nickel-cobalt mixture.

The X-ray emission spectrum of the carbon nanoparticles composing the inner part of the deposit corresponds to the theoretical spectra for the tubes having the structures close to  $(n, 0)$ . The X-ray spectrum of the "light soot" - single-wall closed tubules, produced in the gas phase of the reactor of the arc vaporization of graphite is in better agreement with the theoretical spectra of tubes close to  $(n, n)$ .

## Acknowledgements

This work is supported by the Program "Modern directions in physics of condensed states", on the directions "Fullerenes and atomic clusters", N 94055 and "Surface atomic structures", N 95-2.11.

## References

- [1] S.Iijima, *Nature*, 354 (1991) 56.
- [2] Y.Ando, S.Iijima, *Jpn. J. Appl. Phys.*, 32 (1993) L107.
- [3] X.Sun, C.-H.Kiang, M.Endo et al., *Phys. Rev.*, B54 (1996) R12629.
- [4] A.V.Okotrub, D.A.Romanov, A.L.Chuvilin et al., *Phys. Low-Dim. Struct.*, 8/9 (1995) 139.
- [5] T.W.Ebbesen, P.M.Ajayan, *Nature*, 358 (1992) 220; M.Endo, K.Takeuchi, S.Igarashi et al., *J. Phys. Chem. Solids*, 54 (1993) 1841; M.Ge, K.Sattler, *J. Phys. Solids*, 54 (1993) 1871; M.Ge, K.Sattler, *Mat. Res. Soc. Symp. Proc.*, 349 (1994) 313.
- [6] Z.Ya.Kosakovskaya, L.A.Chernozatonskii, E.A.Fedorov, *Pis'ma v ZhETF*, 56 (1992) 26.
- [7] S.Iijima, *MRS Bulletin*, (November), (1994) 43.
- [8] A.Thess, R.Lee, P.Nikolaev et al., *Science*, 273 (1996) 483.
- [9] L.-C.Qin, S.Iijima, H.Kataura et al., *Chem. Phys. Lett.*, 268 (1997) 101.
- [10] S.Sawada, N.Hamada, *Solid State Commun.*, 83 (1992) 917.
- [11] P.Nikolaev, A.Thess, A.G.Rinzler et al., *Chem. Phys. Lett.*, 266 (1997) 422.
- [12] J.E.Fischer, H.Dai, A.Thess et al., *Phys. Rev.*, B55 (1997) R4921.
- [13] Y.H.Lee, S.G.Kim, D.Tomanek, *Phys. Rev. Lett.*, 78 (1997) 2393.
- [14] R.A.Jishi, L.Venkataraman, M.S.Dresselhaus, G.Dresselhaus, *Chem. Phys. Lett.*, 209 (1993) 77; P.J.Lin-Chung, A.K.Rajagopal, *J. Phys.: Condens. Matter.*, 6 (1973) 3697.
- [15] M.S.Dresselhaus, G.Dresselhaus, R.Saito, *Solid State Commun.*, 84 (1992) 201; C.L.Kane, E.J.Mele, *Phys. Rev. Lett.*, 78 (1997) 1932.
- [16] N.Hamada, S.Sawada, A.Oshiyama, *Phys. Rev. Lett.*, 68 (1992) 1579; J.W.Mintmire, D.H.Robertson, C.T.White, *J. Phys. Solids*, 54 (1993) 1835.
- [17] J.W.Mintmire, B.I.Dunlap, C.T.White, *Phys. Rev. Lett.*, 68 (1992) 631.
- [18] X.Blase, L.X.Benedict, E.L.Shirley, S.Louie, *Phys. Rev. Lett.*, 72 (1994) 1878.
- [19] A.A.Lucas, P.H.Lambin, R.E.Smalley, *J. Phys. Chem. Solids*, 54 (1993) 587.
- [20] M.J.S.Dewar, W.Thiel, *J. Am. Chem. Soc.*, 99 (1977) 4899.
- [21] J.J.P.Steward, *J. Comp. Chem.*, 10 (1989) 209.
- [22] M.W.Schmidt, K.K.Baldrige, J.A.Boatz, et al., *J. Comput. Chem.*, 14 (1993) 1347.
- [23] D.Tomanek, M.A.Schluter, *Phys. Rev. Lett.*, 67 (1991) 2331; D.Tomanek, S.G.Louie, *Phys. Rev.*, B37 (1988) 8327.
- [24] A.V.Okotrub, Yu.V.Shevtsov, L.I.Nasonova et.al., *PTE*, 1 (1995) 193.
- [25] A.V.Okotrub, Yu.V.Shevtsov, L.N.Mazalov et al., *Mol. Mat.*, 7 (1996) 75.

- [26] A.V.Okotrub, Yu.V.Shevtsov, L.I.Nasonova et.al., *Neorganicheskii materialy*, 32 (1996) 974; A.V.Okotrub, A.L.Chuvilin, Yu.V.Shevtsov et al., in *Recent Advances in Chemistry and Physics of Fullerenes and Related Materials*, ed. by R.S.Ruof, K.M.Kadish, 2 (1995) 678.
- [27] A.V.Okotrub, V.D.Yumatov, L.N.Mazalov et al., *Zhurn. Struktutn. Khimii*, 29 (1988) 76 (in Russian).
- [28] R.Manne, *J. Chem. Phys.*, 52 (1970) 5733. D.S.Urch, *J. Phys.*, C3 (1970) 1275; L.N.Mazalov, V.D.Yumatov, V.V.Murakhtanov et al., *X-ray spectra of molecules*, Nauka, Novosibirsk (1977), (in Russian).
- [29] A.A.McFarlane, *Carbon*, 11 (1973) 73; E.Z.Kurmaev, S.N.Shamin, K.M.Kolobova, S.V.Shulepov, *Carbon*, 24 (1986) 249.
- [30] E.-K.Kortela, R.Manne, *J. Phys. C: Solid State Phys.*, 7 (1974) 1749.
- [31] M.R.Pederson, J.Q.Broughton, *Phys. Rev. Lett.*, 69 (1992) 2689.